2015

Construction and Optimization of a Tapered Amplifier System for Applications in Ultra-Cold Plasma Research

Ryan Cole
Colby College

CONSTRUCTION AND OPTIMIZATION OF A TAPERED AMPLIFIER SYSTEM FOR APPLICATIONS IN ULTRA-COLD PLASMA RESEARCH

Ryan Cole

Colby College
Department of Physics and Astronomy
Senior Honors Thesis

Advisor: Dr. Duncan Tate
Submitted: 13 May 2015

ABSTRACT

The number density of cold atoms confined in a magneto-optical trap (MOT) is critically dependent on the intensity of the lasers used to cool the sample. To generate large optical powers while retaining the practicality of homemade external cavity diode lasers (ECDLs), a tapered amplifier (TA) system was designed and constructed to amplify the output of an existing 780 nm, continuous-wave ECDL. The amplifier's performance is discussed in terms of its gain and power output. Under standard operating conditions, optical amplification of 12 dB is achieved, with a maximum power output of 0.75 W. The completed amplifier is installed into an existing MOT at Colby College, and its effect is analyzed in terms of the number density of trapped samples of rubidium-85. MOT measurements are given demonstrating an increase in these number densities by a factor of ten. We conclude with initial results to quantify the amplifier's effect on the dynamics of ultra-cold plasmas created from the trapped atom samples.

ACKNOWLEDGEMENTS

First and foremost, I would like to thank my advisor, Dr. Duncan Tate, for his patience and support throughout this project. Duncan has dedicated so much of his time to making sure that my thesis is a success, and was always more than willing to spend extra time in the lab helping me understand the various elements of the project. I am sincerely thankful for his generosity and guidance.

I would also like to thank Professor Charles Conover for designing and constructing the shutter mechanism used in this project. His willingness to share his work was crucial for the completion of the TA system.

Additionally, I would like to acknowledge the Colby College Department of Physics and Astronomy as a whole. All of the professors within the department have spent enormous amounts of time helping me, both inside and outside of the classroom. Whether it was a question on a problem set, or a job I was considering, each professor has always taken the time out of their day to help in whatever way they can. I feel very lucky to have been a part of this department during my four years at Colby.

Problem sets are a big part of being a physics major. They can be rewarding and immensely frustrating, and at many times they are both. I was lucky enough to have a great group of friends with whom I could share these ups and downs. Many good memories were made in the Physics Conference Room between the hours of midnight and 2 a.m. While I may not always remember the Hamiltonian for a quantum simple harmonic oscillator, and I will always remember these times spent "working" on our homework.

Finally, I would like to thank my mother. Without her support and encouragement throughout my college experience, none of this would have been possible.

TABLE OF CONTENTS

CHAPTER 1: INTRODUCTION TO ULTRA-COLD PLASMAS

1.1 THE PLASMA STATE

What are the states of matter? This question is easy, or at least it seemed easy in high school. There are three states of matter: gas, solid, and liquid. This is an idea reinforced throughout many high school physics, chemistry and earth science classes. It is, however, not true. A fourth state of matter exists in the form of plasma. Plasmas are as common as the flame coming out of a lighter, or a bolt of lightning on a summer night, but can be as exotic as the center of the sun or the interstellar medium in our galaxy. In fact, plasmas are so common that, of the 5% of the universe that humans can see (the other 95% consists of dark matter and dark energy), 99% of that matter is in a plasma state [1,2].

Simply put, a plasma is an ionized gas within which free electrons and ions exist side-by-side [3]. Because the energy required to ionize a substance is generally very high, and to be self-sustaining against recombination, most plasmas are very hot, with temperatures exceeding 1000 Kelvin. That being said, modern laser systems and trapping techniques have allowed for the creation of transient plasmas at the opposite end of the temperature spectrum, with temperatures below 1 Kelvin. In this regime, many basic phenomena related to the plasma state of matter can be investigated [4]. The work presented in this paper will concern these, ultra-cold plasma states.

1.2 TRAPPING AND COOLING ATOM SAMPLES

Ultra-cold plasmas are traditionally created by manipulating atom samples that have been cooled and confined in a magneto-optical trap (MOT). For this reason, a brief discussion of the

methods by which atoms are trapped and cooled is necessary to explain the creation of such a plasma state.

At a fundamental level, atoms are cooled due to the interaction between light and matter. It is well understood that atoms can absorb photons when the photon energies match that of an atomic transition. During an absorption, photons transfer their momenta, $p = 2\pi\hbar/\lambda$, to the atom. This momentum transfer creates a recoil force in the atom, and subsequently changes it's velocity [10]. This phenomenon is the basis for laser cooling experiments. By repeatedly transferring momentum to an atom in a controlled fashion, the atom can be slowed and thus reduced to a very low temperature. Additionally, by detuning the cooling lasers from the natural frequency of the transition, only atoms moving towards the laser beam will see the correct, Doppler-shifted frequency and absorb a photon. When applied in three dimensions, this method, called optical molasses, has been demonstrated to create clouds of cold atoms. That being said, because the cooling mechanism relies on a Doppler shift, the effect is solely dependent on the velocity of atoms in the sample [11]. For this reason, an optical molasses experiment is not capable of spatially restricting a cold atom sample. In order to both cool and trap a cloud of atoms, a magneto-optical trap (MOT) must be used.

A magneto-optical trap (Figure 1) relies on both photon absorptions and an external,

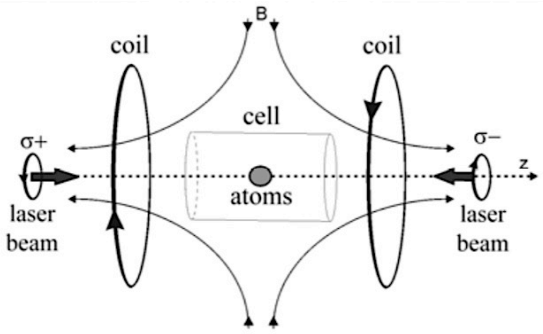

Figure 1.1: Schematic of a MOT [10].

inhomogeneous magnetic field to cool and confine an atomic sample [11]. For simplicity, the functionality of a MOT can be discussed by considering a magnetic field which varies in one dimension, and its effect on how a two level atom with states described by *J=0* and *J=1* absorbs photons [10,11]. According to atomic selection rules, the value of the magnetic quantum number, m_J, is 0 for the *J=0* state and 0, ±1 for the *J=1* state. Additionally, the inhomogeneous magnetic field causes a shift

$$\Delta E = g_J \mu_J B m_J, \qquad (1.1)$$

in the atomic energy levels due to the Zeeman effect, where g_J is the Lande factor, μ_B is the Bohr magneton, B is the magnitude of the magnetic field, and m_J is the magnetic quantum number [10]. Thus, the energy levels in the atom are shifted by an amount proportional to both the magnetic field at the atom's location in space and the m_J quantum number. A schematic of the energy levels for this simplified model is given in Figure 2.

In the context of the model, two circularly polarized laser beams, σ_+ and σ_- are injected

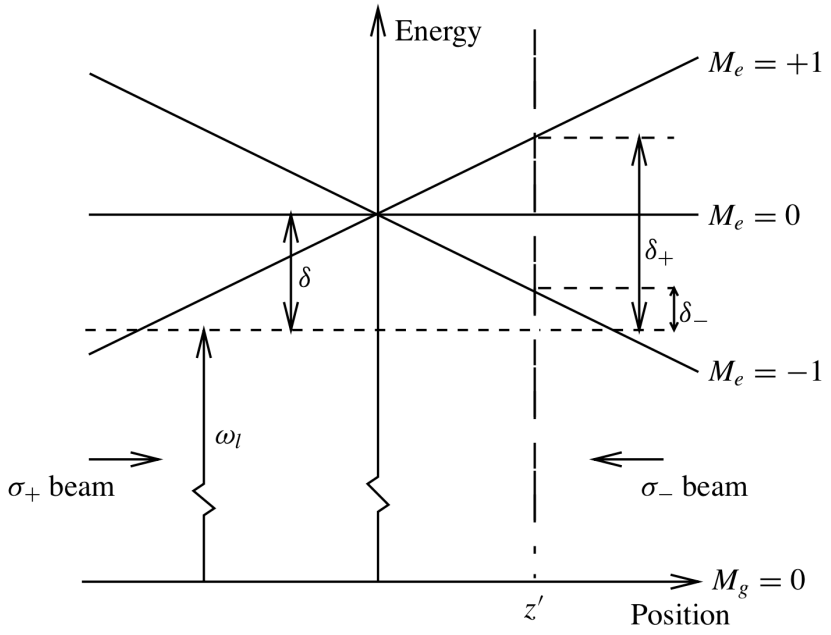

Figure 1.2: Schematic of the MOT energy states. ω_l is the laser frequency, and $\delta_\pm$ represents the relative detuning of each cooling beam [11].

into the MOT. σ_+ is injected from the left, and σ_- is injected from the right, with a circular polarization opposite σ_+. Due to the polarizations, σ_+ drives a transition from the $m_J=0$ to the $m_J=1$ state, while σ_- drives a transition to the $m_J=-1$ state [11]. At this point, the system behaves analogously to an optical molasses configuration. Since the cooling lasers σ_+ and σ_- are detuned below to the resonant frequency of the transitions for a stationary atom, atoms with a certain velocity observe the correct frequency and are slowed. It is important to note, however, that the phenomenon is now position dependent, as the relative detuning of the cooling laser from the transition frequency varies in space with the magnetic field (see Figure 2). Once an atom is sufficiently cold, the force between the magnetic field and the atom's dipole moment begins to dominate over the force due to photon absorptions. The magnetic force pushes the atoms down the magnetic field gradient towards the center of the MOT, thus creating an atom sample that is both cooled and confined [10].

A full quantum mechanical treatment of the forces felt by a particle in the MOT, which is beyond the scope of this thesis, can be used to show that the scattering force felt by each atom in the trap is given by

$$F_s = \frac{\hbar k \Gamma}{2 I_s} \frac{I}{\left[1 + \frac{I}{I_s} + \left(\frac{2\delta}{\Gamma}\right)^2\right]}, \qquad (1.2)$$

where I is the intensity of the laser used to cool the sample, I_s is the saturation intensity, Γ is the scattering rate, and δ is the detuning of the cooling laser [5]. While the details of Equation 2 are not particularly relevant in this context, it is crucially important to note that the scattering force is directly proportional to the intensity of the cooling laser. This fact implies that increasing the optical power of the cooling laser can allow for the creation of denser trapped atom samples.

1.3 ULTRA-COLD PLASMAS

Ultra-cold plasmas are created by ionizing atom samples that have been cooled and confined in a magneto-optical trap. The ionization occurs in a two-step process. First, the cooling laser excites a number of atoms in the cloud into the upper state of the cooling transition, and then a pulsed dye laser completely photoionizes the atoms in the upper state [4]. After the photoionization, the atom cloud exists as a collection of electrons and positive ions, and thus is a plasma. The plasma cloud is held together by the Coulomb attraction between the electrons and positive ions, and thus exists (temporarily) in a stable state.

Following the creation of the initial plasma cloud, a number of dynamical processes take place, which are the subject of discussion later in this thesis. Immediately after photoionization, the plasma goes through a brief period of heating. This heading is due to a process called three-body recombination. Recombination of the electrons and ions in the plasma is generally prevented because the electrons have too much energy to by captured by the positive ions. However, when two electrons come sufficiently close to a positive ion, the excess energy in one electron can be transferred to the other, allowing the cation and the less-energetic electron to recombine. The net result of this process is the production of a large number of energetic electrons. These high-energy electrons can be thought of as a heating mechanism, and cause a brief period of increasing temperature after photoionization.

Once equilibrium is reached after three-body recombination, the plasma cloud begins a phase of expansion. In the process of photoionization, the pulse from the dye laser causes a small amount of energetic electrons to be ejected from the plasma cloud. To a first approximation, the plasma is electrically neutral after it is created, but in reality the absence of the ejected electrons creates a very slight net positive charge. While the plasma itself is held together by the attraction

between the ions and electrons, the net Coulomb repulsion due to the slight positive charge causes the plasma to slowly expand. As the expansion slowly progresses, the distance between the ions and the electrons increases, and consequently the potential well created by the Coulomb attraction becomes shallower and shallower. As the well becomes shallower, more and more electrons are able to escape the plasma, and the net positive charge of the cloud increases. This phenomenon quickly compounds, and the plasma expands faster and faster until it effectively disappears.

The dynamics discussed in this section can be measured by detecting charged particles, either ions or electrons, as they leave the plasma cloud. While other methods of measuring plasma dynamics and characteristics exist, a large regime of physical processes can be studied by simply measuring charged particles emitted from an ultra-cold plasma [4]. The data and discussions presented later on this paper will focus on the direct observation of electrons as they escape the plasma cloud.

1.4 The Lifetime of an Ultra-Cold Plasma

Assuming the photoionizing laser pulse ionizes a certain percentage of the atoms in the MOT, increasing the number densities in the trap (per Equation 2) results in a greater number of ionized rubidium atoms. For this reason, the density of an ultra-cold plasma is expected to increase with the density of the initial trapped sample. The resulting increase in plasma density is suspected to have measurable effects on the plasma dynamics following photoionization.

A major effect of the increased plasma density is likely an increased lifetime of the plasma cloud. If the plasma density increases, the potential well due to the Coulomb attraction between ions and electrons in the plasma will become deeper. This fact would cause the

expansion process to slow, as the Coulomb force is more effective at binding the electrons and ions. The lifetime of plasma state is typically measured by the point at which the expansion process completely destroys the cloud. Thus, if the expansion slows, the measured lifetime should increase.

It is important to note that, under these hypotheses, the lifetime of an ultra-cold plasma can be tied to the optical power of the lasers used in the MOT. For this reason, increasing plasma lifetimes can be thought of as the overarching experimental goal for this thesis.

CHAPTER 2: TAPERED AMPLIFIERS

2.1 THE TAPERED AMPLIFIER

As discussed in Section II, the atomic scattering force, and thus the density of atoms confined in a magneto-optical trap (MOT), is critically dependent on the intensity of the laser used to cool the sample. While external cavity diode lasers (ECDLs) are commonly used because of their cost-effectiveness and precision, these lasers are often only capable of producing output powers of less than 100 mW [6]. For this reason, an amplifier that produces large optical gains while preserving the narrow linewidth of the ECDL is essential for cooling large samples of atoms. The tapered amplifier (TA) is a common device used for this effect.

The design and functionality of the tapered amplifier can be discussed in terms of a simplified model [5,6]. For the purposes of this discussion, the design of the amplifier chip itself can be thought of as consisting of two components: a waveguide and a tapered gain region. Light from the ECDL (the "seed laser") enters the amplifier through an anti-reflection coated facet, and

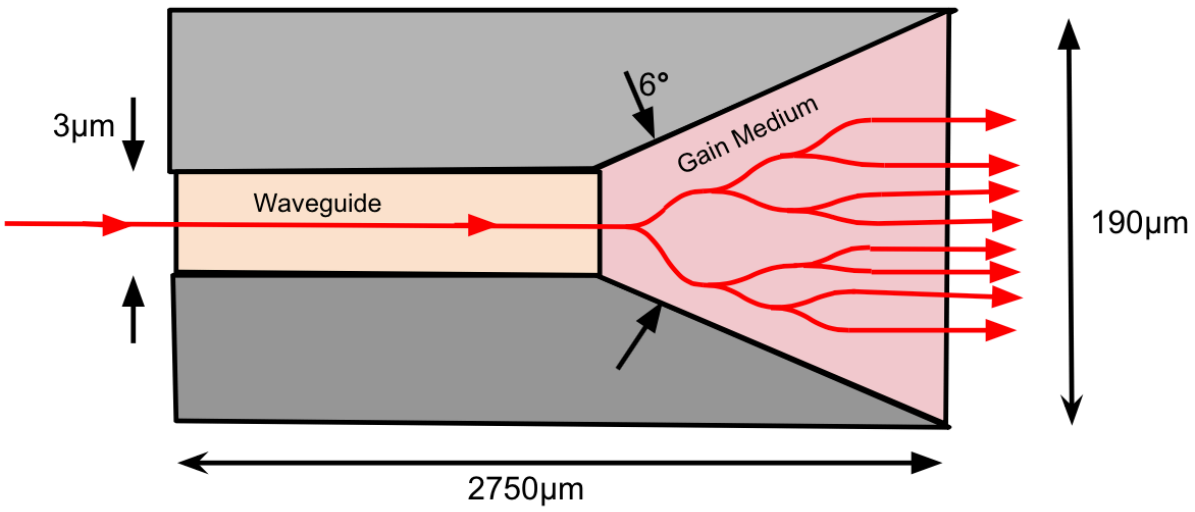

Figure 2.1: Schematic of the tapered amplifier chip.

fills the waveguide. The input facet on the waveguide is only 3 μm wide, which allows small amounts of input power to create large energy densities within the waveguide [5]. After propagating down the waveguide, the seed light hits the tapered region, and diffracts to completely fill the gain region. This region is uniformly pumped by an external current, which provides the energy to facilitate amplification. A schematic of the tapered amplifier chip is given in Figure 2.1.

2.2 TAPERED AMPLIFIER THEORY

To discuss the process by which a seed photon is amplified, the gain medium can be considered as a two-state system, with lower state $|A\rangle$ and upper state $|B\rangle$ [1,2]. When the medium is pumped by a driving current, electrons in the state $|A\rangle$ are excited into the upper state $|B\rangle$. Through this process, a population inversion is created in which more electrons are found in the upper state than in the lower. Once in the upper state, electrons can decay back to the $|A\rangle$ state by means of spontaneous or stimulated processes [5]. When an electron is in the $|B\rangle$ state, it can stochastically decay to the $|A\rangle$ state and emit a photon. Because the emitted photon is not causally linked to the seed photons, the mode of the two photons does not necessarily match [5]. Conversely, when the system is in the $|B\rangle$ state, a photon from seed laser can stimulate a decay to the $|A\rangle$ state, again emitting a photon. Since the seed photon stimulates the creation of the second photon, the two photons must have identical modes. This guarantees that the frequency, direction of propagation, and polarization of the two photons are identical [5]. The net result of this process is the creation of two photons from a single seed photon. A schematic of these processes is given in Figure 2.2.

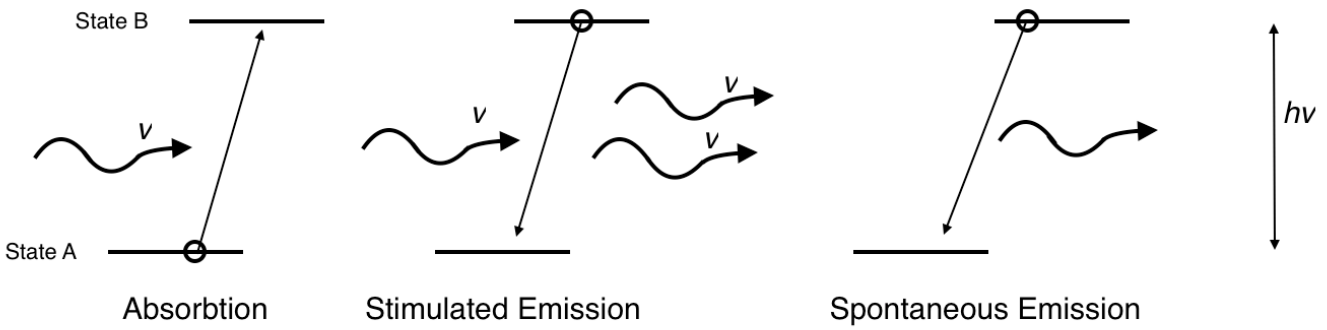

Figure 2.2: Energy level diagram showing the processes involved in the two-level model of the tapered amplifier.

The photons involved in either the stimulated or stochastic processes continue to propagate through the gain medium, and are free to stimulate further transitions and emissions. However, since photons produced in stimulated emission match the mode of the seed laser, they can be considered the only useful product of the amplification process. As these photons propagate through the gain medium, they create an "avalanche" of identical photons all created from a single incident particle. This "avalanche" effect is the mechanism by which the tapered amplifier amplifies incident light.

It is important to note that the two-state system presented in this section is somewhat of an over simplification. In a more realistic model, this system should consist of four states: a base state, a reservoir state, and states $|A\rangle$ and $|B\rangle$. Electrons in the base state are excited to the reservoir state by the driving current. From this state, they decay to the $|\mathrm{B}\rangle$ state, where either the stimulated or stochastic process can cause the electron to decay and produce a photon, as described above. Once in the $|A\rangle$ state, the electrons decay further back to the base state. At this point, the electron can be excited back to the reservoir state, and the cyclic process repeats. In both the two-state and four-state models, it is necessary that state $|B\rangle$ has a much longer lifetime than state $|A\rangle$. This fact both allows for a population inversion to be created, and it minimizes the amount of (useless) stochastic emissions relative to mode-matching stimulated emissions.

The simplistic model presented in this section is far from a complete treatment of the physical processes at work in a tapered amplifier. While two-level atomic transitions in the TA chip do not actually occur, considering an analogous effect in the bulk matter within the TA chip provides for a good model of the chip's functionality. More detailed, semiconductor-based discussions can be found elsewhere [5,6,8].

CHAPTER 3: EXPERIMENTAL I

3.1 TA DESIGN AND CONSTRUCTION

The overall construction of the tapered amplifier housing described in this paper was largely completed before the inception of this project. That being said, a description of the TA chip and housing construction will be relevant to explain many of the methods and results presented in this paper.

The amplifier relies on a model EYP-TPA-0780 tapered amplifier chip produced by Eagleyard Photonics. The chip itself is mounted to a C-mount [5], which, in turn, is secured to a larger aluminum block. This collection is then secured atop a set of larger aluminum baseplates that both raise the chip to an appropriate height above the optical table and serve as a heat sink for the device. Because the TA chip generates a significant amount of heat during operation [6], a set of thermoelectric coolers are attached at the interface between the aluminum mounting and the baseplate. Both the TA chip and the thermoelectric coolers are driven by a ThorLabs ITC4000 Laser Diode and Temperature Controller.

Eagleyard Photonics specifies that the input facet of the TA chip is 3 μm wide, so careful considerations must be taken to focus the seed laser into the chip. To account for this, an aspherical lens is permanently mounted on the input side of the TA housing. The lens is attached to a 3-dimensional, translational stage, which allows the position of the lens focus relative to the input and output facet to be finely adjusted. Additionally, due to the geometry of the chip itself, the output of the amplifier is highly divergent. To correct for this, an identical aspherical lens is mounted on the output side of the chip to collimate the light leaving the amplifier. Images of the assembly are given in Figures 3.1 and 3.2.

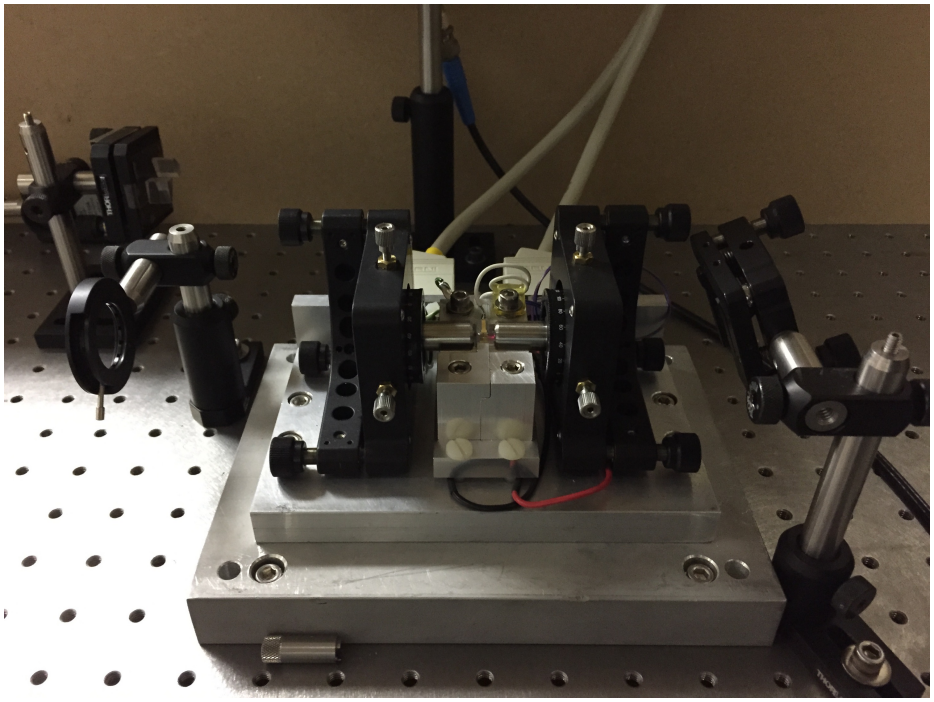

Figure 3.1: An image of the TA housing with protective Plexiglass cover removed. Elements of the optical setup (a pinhole and cylindrical lens) are also visible in the image.

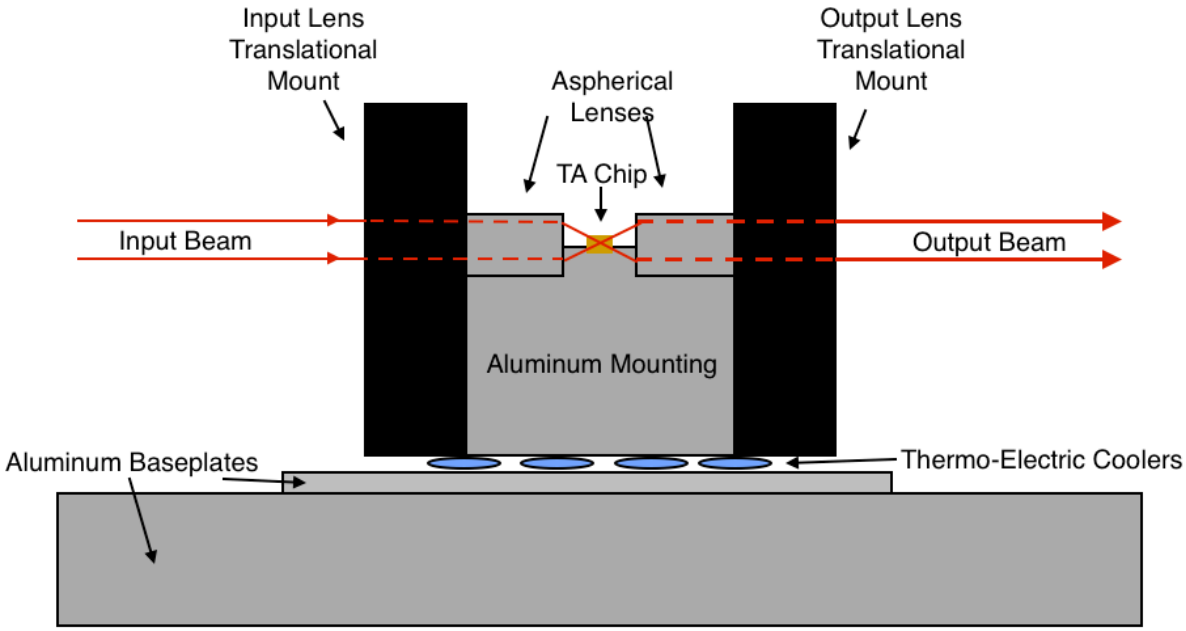

Figure 4.2: A schematic showing the important components of the TA housing.

3.2 Optical Setup for Optimization

Once the tapered amplifier was constructed and operational, an optical configuration was designed to investigate and optimize the properties of the tapered amplifier. The optical design consisted of four major components: a saturated absorption spectrometer, pre-TA optics, post-TA optics, and a set of interlocks designed to protect the TA itself. The entire arrangement was built around a homemade, 780nm, external-cavity diode laser (ECDL), which would provide the seed beam to power the TA. An overview of the optical configuration is given in Figure 3.3.

While the saturated absorption spectrometer was not essential for the operation of the tapered amplifier, it did facilitate the observation of the $5S_{1/2} \rightarrow 5P_{3/2}$ transition for rubidium-85. The $5S_{1/2} \rightarrow 5P_{3/2}$ transition is cyclical, and thus serves as the primary transition used to cool ^{85}Rb samples. Observation of the cooling transition using the saturated absorption spectrometer

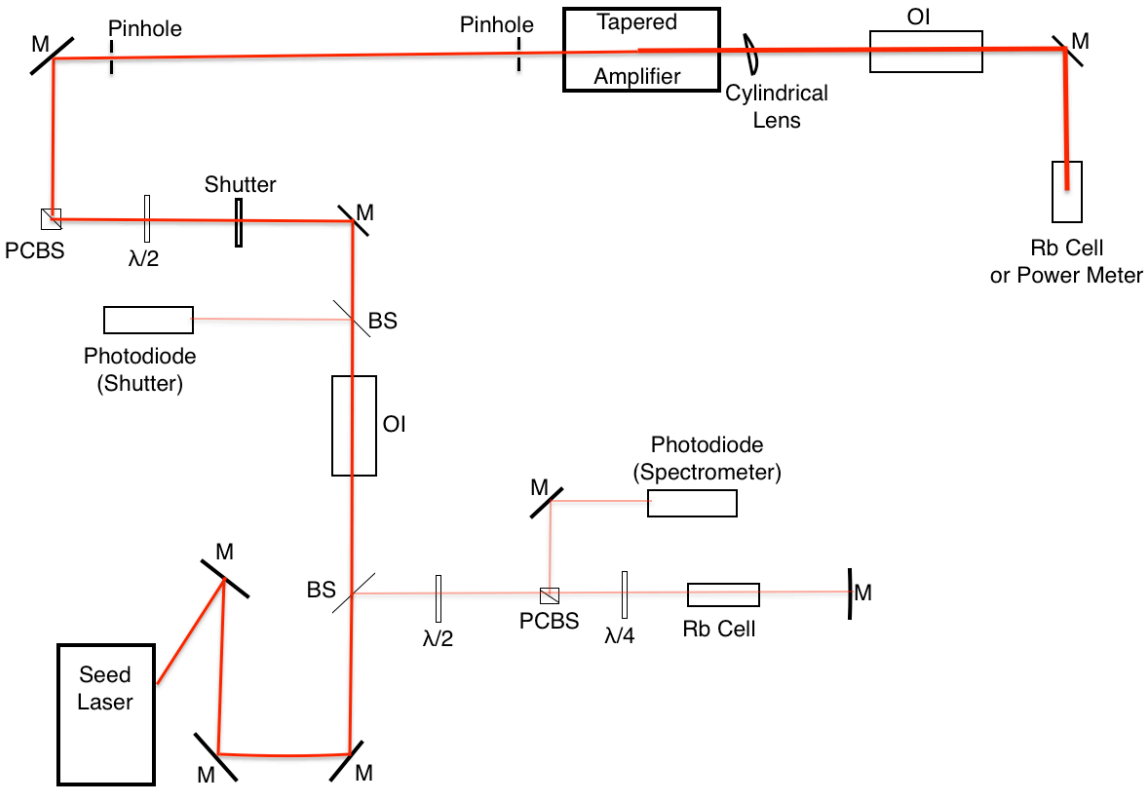

Figure 5.3: A schematic of the optical setup used to optimize the TA. "M" signifies a mirror, "BS" a beam splitter, "PCBS" a polarizing cube beam splitter, "OI" an optical isolator, and "λ/2" a half-wave plate.

allowed for verification that the output of the ECDL was adequate for the trapping and cooling of rubidium. Furthermore, using an infrared camera, fluorescence due to the transition could be observed in the rubidium cell. This fluorescence proved to be an important feature for qualitatively evaluating the output of the tapered amplifier, as will be discussed in a later section.

Aside from the spectrometer, the rest of the optical configuration was devoted directly to the operation of the TA and measurement of its properties. On the input side of the TA, the device is very sensitive to both the alignment and power of the seed beam. Because of this, careful consideration was taken to allow for fine adjustment of the beam aiming and power. Beam alignment was achieved using a "steering" mirror, a polarizing cube beam splitter (PCBS), and a set of pinholes. Using these components, the precise path to the 3 μm input facet of the TA chip could be marked by the pinholes, and the seed beam could be directed down the path using the PCBS and steering mirror. Furthermore, a λ/2 plate placed the before the PCBS could be adjusted to vary the amount of power directed towards the amplifier.

As previously mentioned, the geometry of the TA chip causes its output to be highly divergent. While this issue is partially accounted for using the aspherical lenses discussed in Section 3.1, the amplified light following the lens remains highly astigmatic in one dimension. To correct for the astigmatism and provide a circular output beam, a cylindrical lens must be used to collimate the beam in the dimension unaffected by the aspherical lens. Due to the proximity of the lens to the output of the TA, the lens was mounted at a sharp angle relative to the amplifier. This consideration reduced the chance of a retro-reflection that could damage the chip [6,8]. To further protect against retro-reflections, the amplified beam is injected into an optical isolator (Conoptics Model 714), which blocks any light that would be travelling the wrong direction into the output of the TA.

3.3 INTERLOCK SYSTEM

To maximize the lifetime of the TA chip, the amplifier should only be used when the driving current is on and the seed beam is incident. The TA chip is at risk of damage if it is operated without a seed beam, or if the seed beam is left incident on the chip in the absence of a driving current [6]. To make sure these conditions are met, a set of interlocks were designed to ensure the amplifier is operated under the appropriate conditions. The interlocks largely take advantage of the settings available on the ThorLabs ITC4000 controller, which supplies the driving current to the TA and controls the TEC system.

To ensure the TA is only powered when the seed laser is on, a photodiode was used to detect light from the seed beam. The photodiode signal was shaped to a TTL signal using a Schmitt Trigger circuit. This signal was fed to the TA controller, which would only enable a current to the TA if a TTL+5 signal was received from the diode. Additionally, to ensure that the seed laser is only incident upon the amplifier when the TA is powered, a shutter was built using a repurposed computer hard drive to block and unblock the seed beam when appropriate. The construction of the shutter device and controller followed the work of reference [7], and was completed prior to the beginning of this project. The ThorLabs ITC4000 controller was programmed to drive the shutter so that the seed beam is unblocked if and only if a current is flowing to the TA.

As a final element to the interlock system, the temperature controller component of the ITC4000 was set to stop any current flowing to the TA if the chip temperature left a pre-set window. Per the suggestion of references [5] and [6], this temperature window was set to be 18.00 ± 2.00 C. The combination of the temperature interlock with the current and seed beam

interlocks function well to satisfy the above-mentioned conditions as well as to prevent any unnecessary stress or damage to the TA chip.

3.4 TA ALIGNMENT PROCEDURE

Due to the precision with which the seed laser must be aligned with the TA input facet, even slight bumps to the optical bench or ambient temperature fluctuations can cause the TA to become misaligned. Furthermore, the performance of the amplifier is extremely sensitive to the physical alignment of the seed beam and the input facet. For these reasons, it became very important to have a well-documented, repeatable, and dependable procedure for coupling the ECDL seed beam into the TA chip. The following procedure was developed based upon the suggestions presented in reference [8].

When operated without a seed beam, the TA chip produces light through amplified spontaneous emission (ASE). Due to the chip geometry, this light is extremely divergent, and must be collimated using the aspherical lenses on both the input and output sides of the TA. When properly collimated, the ASE beam is level relative to the optical table, but still has an elongated beam profile that is highly divergent in the plane parallel to the optical bench. While driving the TA with a small current (~200 mA), the ASE emerging from the input facet of the TA chip should be aligned with the two pinholes (refer to Figure 3.3). Using the PCBS and the steering mirror, the seed beam from the ECDL should then be directed though the pinholes, so that it spatially overlaps the ASE beam propagating in the opposite direction. Once alignment is completed, the seed beam should be allowed to enter the TA. While monitoring with a power meter, the seed beam should be blocked and unblocked repeatedly to see if the output power varies with the seed beam. If the output power increases when the seed beam is incident, the seed

and TA are properly aligned. If not, the alignment must be checked and corrected. Once rough alignment is achieved, the amplifier can be optimized by finely adjusting the translational mounts on the TA housing and the steering mirror.

While this procedure was very dependable for aligning the amplifier, re-alignment often resulted in slight power fluctuations in the TA output. Due to the delicate geometry of the TA chip, minute misalignments have a noticeable effect on the TA performance. For this reason, differences in output power of up to ±5% were often observed before and after re-alignment, and should be considered normal.

CHAPTER 4: PERFORMANCE OF THE TAPERED AMPLIFIER

4.1 TA OPTIMIZATION

With the amplifier properly aligned, a FieldMaster FM optical power meter by Coherent, Inc. was used to investigate the power output of the TA. By varying the input power of the seed beam and measuring the output of the TA, a set of input/output power curves were obtained for a number of TA driving currents (Figure 4.1). Under variable input power and driving currents the amplifier was seen to produce between 7 and 470 mW of output power when operated well below the maximum driving current (3 A) quoted by the manufacturer. The power curves were used to investigate the gain and saturation characteristics of the amplifier.

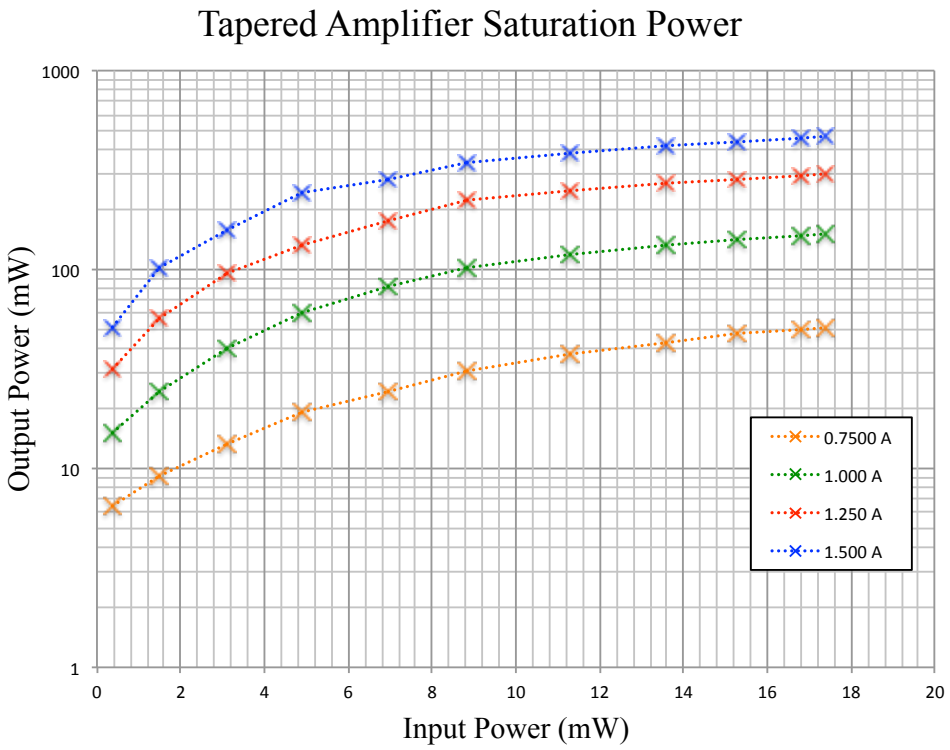

Figure 4.1: Output powers as a function of input power for a number of different driving currents. The TA is well saturated near 10 mW for all currents.

The saturation power of the TA was of particular interest for correct use of the amplifier. The saturation power is the seed power at which the amplifying medium in the TA chip is entirely saturated by the seed light. When the TA chip is operated near its saturation point, the stimulated emission from the gain medium is most efficient, and thus optimized. Furthermore, consistent operation of the amplifier above the saturation power can degrade and damage the TA chip [5]. Figure 4.1 shows that the amplifier is well saturated for all driving currents at approximately 10 mW seed power. Above this power, the increased input power does does not lead to a proportionally larger output power, indicating that the gain medium is fully saturated [9].

Since the TA chip is designed to be operated near the saturation condition, the amplification gain was investigated near this point. Using the data presented in Figure 4.1, the TA gain was observed to vary between 5 and 16 db at a seed power of 8.9 mW, where we have defined gain as

$$G_{db} = 10log\left(\frac{P_{out}}{P_{in}}\right) \qquad (4.1)$$

[12]. As expected, the TA gain is critically dependent on the current that drives the TA (Table 4.1). Eagleyard Photonics quotes a maximum driving current of 3.0 A for the EYP-TPA-0780 TA chip. Because of this, the maximum gain quoted in Table 4.1 is far below the maximum

TA Driving Current (A)	Amplifier Gain (db)
0.7495	4.95
0.9995	9.19
1.2495	12.16
1.4995	14.40
1.7496	15.89

Table 4.1: Measured amplifier gains for variable driving currents.

possible for the chip. However, power output data was only collected at or below a driving current of 1.5 A in an effort to avoid damaging the chip.

Once the power output of the TA was well understood, a quick-check was made to verify the spectral purity of the TA output. As previously stated, the cooling transition in ^{85}Rb must be driven by a laser that is finely tuned to precisely 780 nm. For this reason, any wavelength shift in the TA amplification process would severely limit the amplifiers' ability to drive this transition. While there seems to be no theoretical mechanism that would lead to an alteration of the input wavelength in the amplification process, a quick procedure was used to qualitatively verify this fact. A rubidium cell in the saturated absorption spectrometer was brought into resonance with the $5S_{1/2} \rightarrow 5P_{3/2}$ transition, and fluorescence from the transition was observed using an infrared camera. Next, an additional rubidium cell was placed in the path of the amplified output of the TA. With the cell in place, florescence from the cooling transition was simultaneously observed in the rubidium cells both before an after the amplifier. Using this observation, it can be inferred (at least to a qualitative degree) that the wavelength of the TA output is functionally identical to that of the seed beam.

Now that the amplifier's output properties had been investigated and optimized to a basic level, the device was ready to be integrated into an existing magneto-optical trap (MOT). While additional tests to further understand the output properties of the TA could have been completed (see Chapter 7), the data presented in this section provides a sufficient understanding to successfully implement the amplifier into a trapping and cooling system. The rest of this paper will be devoted to the amplifier's installation and performance in a MOT.

CHAPTER 5: EXPERIMENTAL II

5.1 INTEGRATION INTO THE MOT

Using the optical system presented in Chapter 3, a new optical configuration was designed to integrate the tapered amplifier into an existing magneto-optical trap. Similar to before, the cooling laser in the MOT is build around an ECDL. However, the existing MOT system uses boosting lasers to augment the optical power from the ECDL. This consideration gives the system the capability to produce over 100 mW of optical power before the TA. While the optical design is fundamentally the same as the previous configuration, several nuances were added for future applications in the project. First, because the MOT uses both a cooling and re-

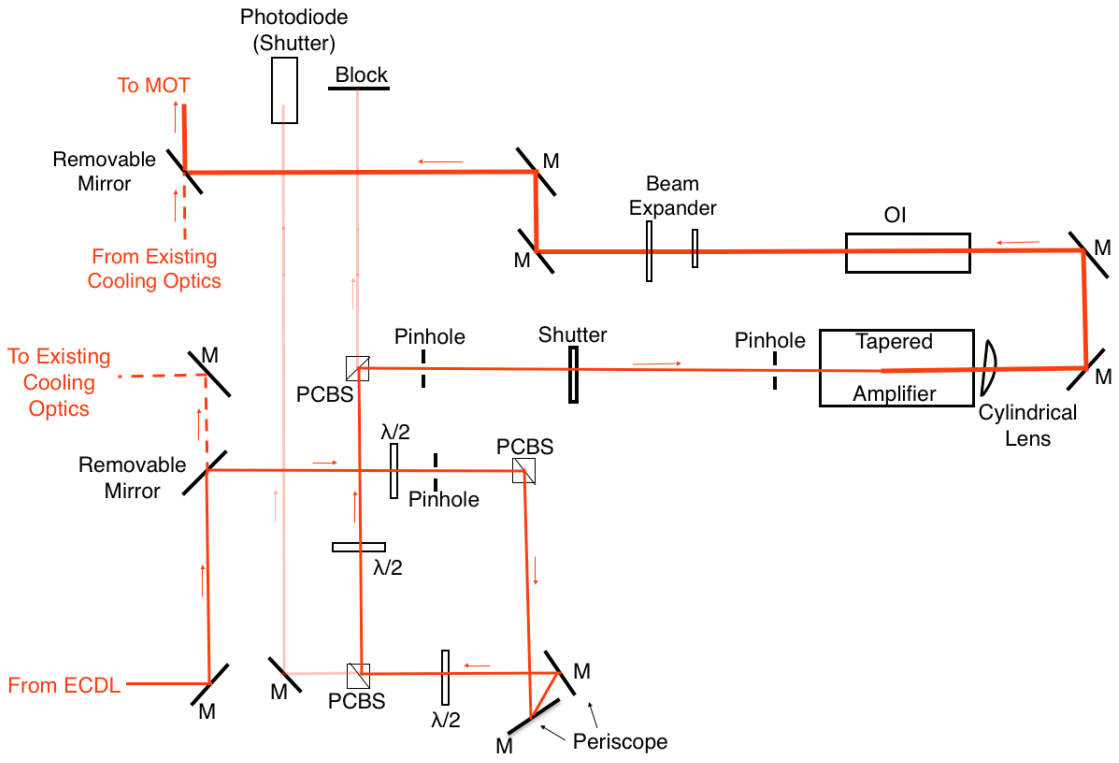

Figure 6.1: A schematic of the optical setup used integrate the TA into the existing MOT at Colby College. Arrows are used to indicate the direction of beam propagation. Nomenclature given in Figure 5.1

pump laser, the new optical configuration was designed to allow for the simultaneous amplification of both lasers. Second, several optical components were carefully chosen so that the MOT can be reverted to its original, non-amplified form without major alterations. These additions do not change the functionality of the design, but do add flexibility for future elements of the experiment.

To allow the TA system to be easily added and removed from the trapping optics, a ThorLabs KS1R removable mirror was used to divert the cooling laser from its original path in the MOT optics to the TA system. This removable mirror was used because it has a repeatability of 10 micro-radians. The ability of the removable mirror to return to its exact position allows the mirror to be removed and replaced without jeopardizing the fine alignment of the amplifier optics. Figure 5.1 gives a schematic of the amplifier optics following the removable mirror. A

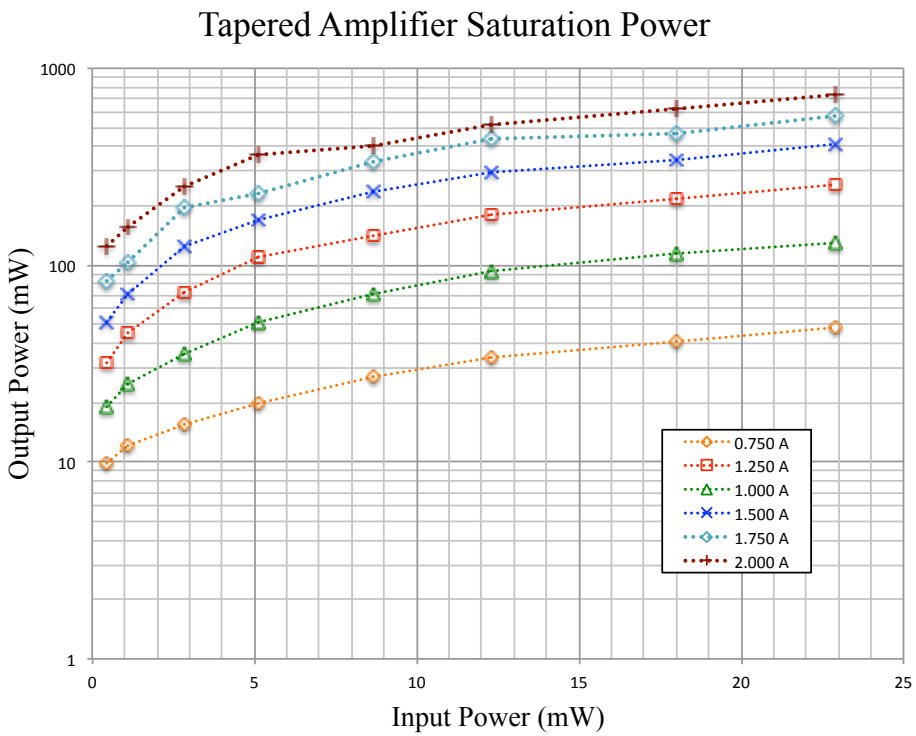

Figure 5.2: Output powers as a function of input power for a number of different driving currents. As before, the TA is well saturated near 10mW for all currents. Data taken after integration into the MOT configuration.

number of polarizing cube beam splitters (PCBS) are used to manipulate the cooling beam and allow the optical power reaching the amplifier to be varied. Furthermore, the cooling and re-pump beams can be injected into a PCBS with orthogonal polarizations to combine light from the two lasers in the path of the amplifier. This allows the TA to simultaneously amplify light from both the cooling and re-pump lasers, which are subsequently directed to the same location in the MOT.

Following the string of beam splitters, the seed beam is coupled into the TA using the optical components discussed in Chapter 3. After the amplifier, the output beam is shaped and expanded by a set of beam expanding lenses to a circular profile roughly 15 mm in diameter. This beam is then directed back into the path of the MOT optics using an additional KS1R removable mirror.

To verify the performance of the TA after the transition into the MOT system, a set of power curves (Figure 5.2) similar those given in Figure 4.1 were collected for the new optical system. Using the understanding of the TA's power output, the driving current was pushed to 2.0 A, which is two thirds the maximum current quoted by the manufacturer. The increased current facilitated a maximum output power of 789 mW, which was the device's maximum observed output power. Analysis of the power curves show that, as expected, there was no performance change in the amplifier due to the new optical design. The data given in Figure 6 is indicative of a saturation power near 10 mW seed power, which is in good agreement with the value given in Chapter 4. Close examination also shows that the output powers quoted for the new optical design are slightly less than the corresponding values in Figure 4.1. This discrepancy is likely due to a slight misalignment of the seed beam into the TA, and normalized once the alignment was improved.

5.2 Creating an Ultra-Cold Plasma

Once trapped, the sample of 85-rubidium was driven to a plasma state using a beam from a 480 nm pulsed Littman laser. This pulse ionizes a percentage of the sample, and the result is a plasma consisting of electrons and rubidium cations. Simultaneously with the photoionization, the magnetic field in the MOT is reduced to allow the plasma dynamics discussed in Chapter 1 to be observed. During this period, a slight electric field is induced to push the charged particles, either ions or electrons, towards the Micro-Channel Plate Detector, which can record the charged particles as they are emitted. The polarity of the external field can be switched to allow the observation of electrons instead of ions, or vice versa. The signal from the Micro-Channel Plate is viewed on an oscilloscope, where analysis of the resulting signal can take place. A schematic of the MOT and detector configuration is given in Figure 5.3.

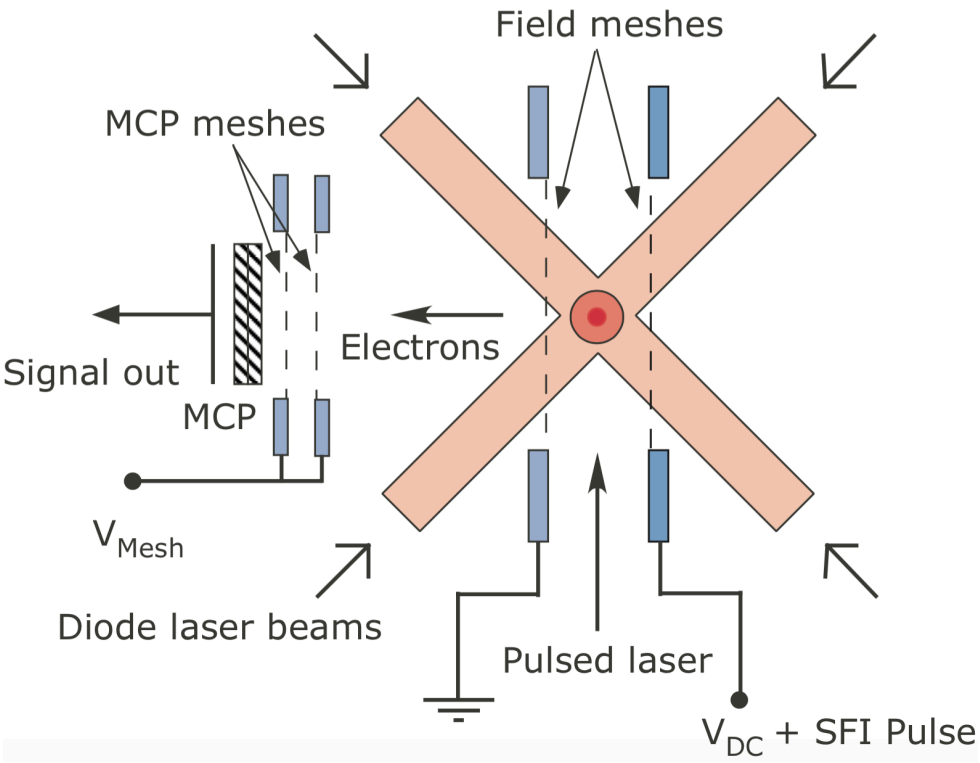

Figure 5.3: Schematic of the MOT, showing the Multi-Channel Plate (MCP) and field meshes used to record the charged particles emitted from the trapped plasma.

CHAPTER 6: RESULTS AND DISCUSSION

6.1 NUMBER DENSITY RESULTS

Once fully aligned with the existing MOT optics, light from the tapered amplifier was used to cool a sample of 85-rubidium in the magneto-optical trap. As expected, the addition of the TA into the MOT optics did not affect the ability to trap and cool atom samples, and a cold atom sample was observed using the output of the TA (Figure 6.1). As discussed in Chapter 1, there is theoretical evidence to suggest that increasing the optical power of the cooling laser allows for the creation of denser trapped atom samples. Thus, the TA's ability to create optical powers in excess of 100 mW (the previous output power of the cooling laser) was expected increase the density of ^{85}Rb samples confined in the MOT.

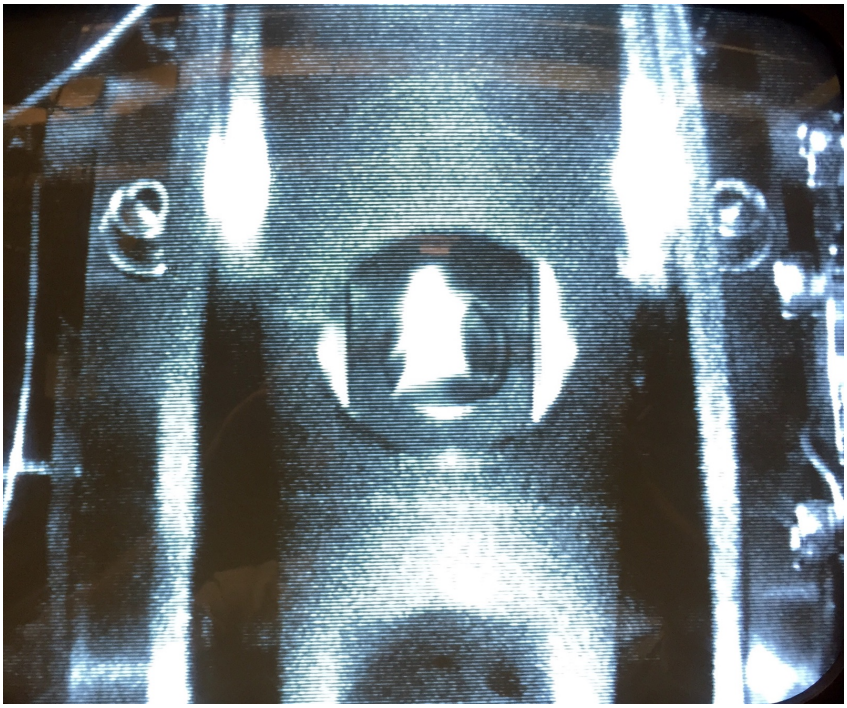

Figure 6.1: A cloud of trapped rubidium in the MOT. Image gathered using an infrared camera.

The number density of atoms confined in the MOT can be inferred from measurements of the fluorescence power emitted from the MOT and the spatial profile of the trapped cloud. The fluorescence power of the trapped cloud was measured by positioning the Fieldmaster optical power meter at one of the windows on the MOT. Fluorescence powers of up 2.7 μW (background corrected) were observed when using the amplified cooling laser. Prior to the installation of the TA, fluorescence powers were seldom observed to exceed 1 μW. The elevated power measurements served as an initial indicator that the TA was indeed facilitating the trapping of denser rubidium samples. In addition to the fluorescence power measurements, a Unidata Linear Diode Array was used to make one-dimensional measurements of the physical size of the trapped atom cloud.

By making the assumption that the trapped atom cloud has a Gaussian spatial profile, the number densities of rubidium-85 atoms trapped in the MOT can be expressed as

$$n_{max} = \frac{N_{atom}}{(2\pi\sigma^2)^{3/2}} \cong \frac{\left(6.47\times10^7\right)P_F}{(2\pi\sigma^2)^{3/2}} \qquad (6.1)$$

and

$$n_{avg} = \frac{N_{atom}}{(4\pi\sigma^2)^{3/2}} \cong \frac{\left(6.47\times10^7\right)P_F}{(4\pi\sigma^2)^{3/2}} \qquad (6.2)$$

where P_F is the florescence power measured by the power meter. The parameter σ^2 is the variance of the Gaussian spatial profile of the atom cloud, which can be related to the full width at half maximum of the signal from the photodiode array. A full derivation of Equations 6.1 and 6.2 is given in Appendix 1.

Using the measurements from the diode array and power meter, a set of number density measurements were made for different cooling laser powers. The resulting data is summarized in Table 6.1. Before the installation of the tapered amplifier system, the maximum observed

Cooling Laser Power (mW)	Measured Number Density (cm^{-1})
100*	1×10^{10} *
160	1.15×10^{11}
239	6.09×10^{10}

Table 6.1: Measured number densities as a function of cooling laser power. Starred values reflect maximum observed densities before installation of TA.

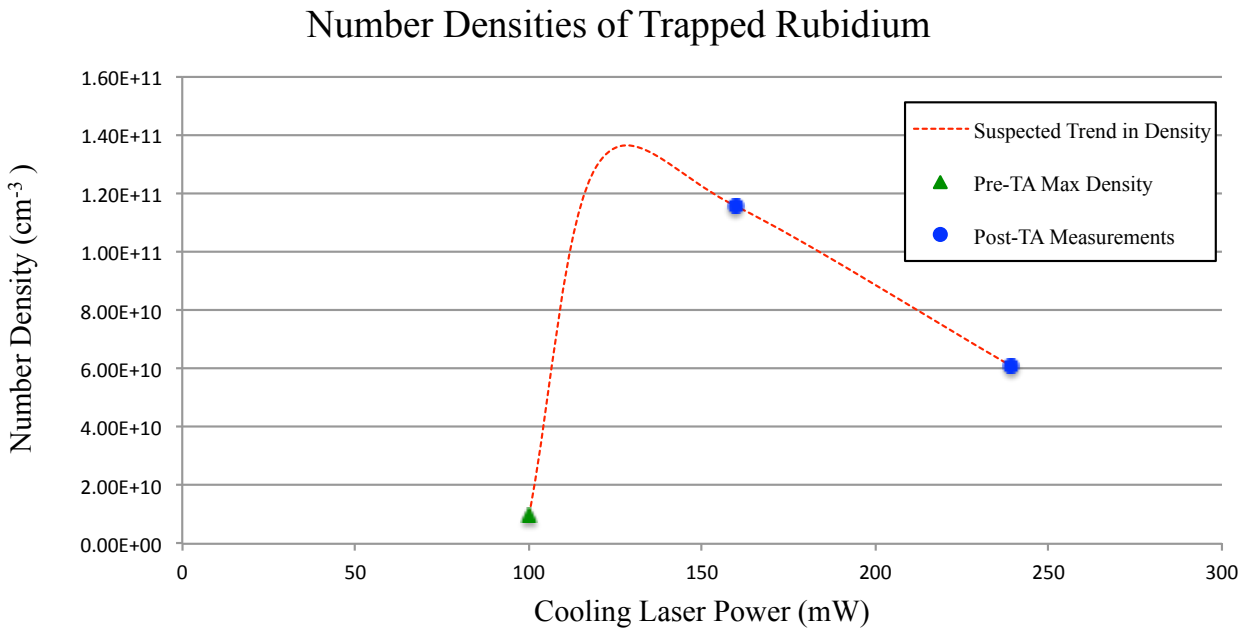

Figure 6.2: Plot of number densities shown in Table 6.1. Red dotted line shows suspected trend in number densities cooling laser power is increased.

number density of rubidium atoms in the MOT was approximately 1×10^{10} cm^{-3}. Thus, as predicted, both values given in Table 6.1 reflect significant increases in the density of trapped samples. Because of this, it is clear that the TA was successful in increasing the density measurements in the MOT That being said, the preliminary measurements given in the table also show that the number density of 85-rubidium decreases as the cooling laser power is increased. For this reason, it is suspected that the number density of trapped atoms reaches a maximum somewhere between cooling laser powers of 100 to 160 mW (see Figure 6.2). Potential causes of the decreasing number density include heating effects at high optical powers, or an inability of the re-pump laser to keep a sufficient number atoms in the state necessary for the cooling transition to take place. At the time of data collection, fluctuating temperatures in the laboratory interfered with laser locking and stability, and prevented a controlled environment under which this phenomenon could be investigated. Further work will be necessary to fully understand the dependence of the number density on cooling laser power.

6.2 Plasma Results

Plasma data recording the number of electrons ejected as a function of time was recorded using the oscilloscope. Since the electrons must travel a distance from the plasma cloud to the Micro-Channel Plate, the resulting signal is called an electron time-of-flight spectrum. However, since the electron can be thought of as having negligible mass, its time taken to travel from the plasma to the detector (the "time of flight") is also negligible. Thus, the times given in the spectrum can be regarded as the instants that the electrons were ejected from the plasma. A time-of-flight spectrum for a plasma created using the TA is given in Figure 6.2.

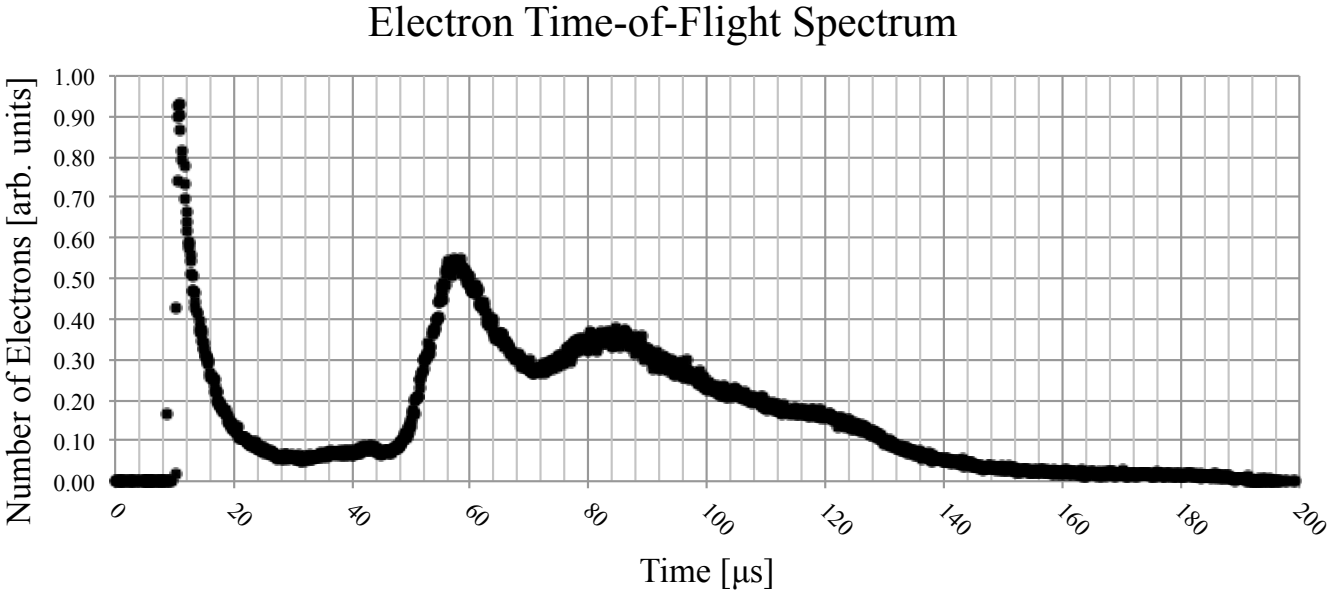

Figure 6.3: An electron time-of-flight spectrum for an ultra-cold plasma created using the TA. Shows a spike due to three-body recombination and a broad hump due to the expansion phase.

Figure 6.3 is a background-subtracted spectrum showing the number of electrons registered by the Multi-Channel Plate (in arbitrary units) as a function of time. In the plot, the photoionizing pulse from the Littman laser occurs at roughly the 10 μs mark, and is followed by a sharp peak in electron counts. This peak is due to the process of three-body recombination, which is discussed in detail Chapter 1. The flux of energetic electrons released in this phenomenon causes the sharp peak in electron counts immediately after ionization.

Following the three-body recombination peak, a broader hump is visible in the spectrum, which is due to the plasma's expansion. As before, the plasma expansion phase is discussed in detail in earlier sections. The signal we measure is the electrons that escape as the plasma becomes more diffuse and the Coulomb force begins to be less effective. By looking at the point at which the signal returns to the zero point, we can determine the point at which the plasma is no longer emitting electrons. This corresponds to the lifetime of the plasma state. Figure 6.3

shows a plasma lifetime of approximately 160 μs, a value that does not reflect an increase due to the introduction of the tapered amplifier system.

Additionally, the time-of-flight spectrum shows several irregular humps on the signal caused by the expanding plasma. Previous observations of plasmas using the MOT have shown that the expanding plasma produces a smooth signal. For this reason, the humps in Figure 6.3 are indicative of irregular plasma dynamics during the expansion phase. While further work will be necessary to investigate the root of these irregularities, several potential causes are likely. After expansion of the TA output, a number of interference fringes were visible in the cooling beam. These fringes can cause power variation in the beam, and subsequently lead to density fluctuations in the trapped atoms. Additionally, it is possible that the amplified spontaneous emission from the TA can create hot electrons in the plasma cloud. Both of these phenomena are capable of causing irregular dynamics in the plasma cloud. As mentioned in Section 6.1, issues with frequency locking and laser stability at the time of data collection, prevented a preliminary investigation into these hypotheses. Further work will be necessary to quantify the cause of the irregular plasma dynamics.

CHAPTER 7: CONCLUSION

7.1 CONCLUSIONS AND FUTURE WORK

This thesis presents the design, optimization, and performance of a tapered amplifier system for applications in laser cooling and ultra-cold plasma research. An effective optical setup for TA operation is presented, and the amplifier is shown to be capable of producing impressive optical output powers by amplifying an existing continuous-wave laser. Additionally, a number of the amplifier's characteristics were investigated, including the gain properties and saturation levels. These simple measurements provide a sufficient understanding to allow for the safe and effective amplification of an existing laser system.

The tapered amplifier system was used to amplify the cooling laser in an existing magneto-optical trap at Colby College. The trapping and cooling of rubidium-85 samples was investigated as a function of cooling laser power. As expected, the TA facilitated the creation of cold atoms samples that were far denser than previous samples collected in the MOT. A photoionizing laser was used to create ultra-cold plasma states out of the trapped atoms. By recording the electrons emitted from the plasma, the effect of the increased number densities on plasma dynamics was probed. The resulting data did not indicate that the elevated number densities increased the lifetime of the plasma state. That being said, irregularities in the plasma spectrum indicate a number of complexities that must be addressed before the plasma lifetime can be further investigated.

In the future, a more detailed investigation of the spectral output of the tapered amplifier could lead to better understanding of the amplifier's effects on trapped atom samples. Specifically, a quantification of the fraction of the amplifier's ASE that lies within a certain fraction of the cooling laser's linewidth could prove beneficial for future experiments.

Furthermore, optical adjustments after the TA are necessary to improve the spatial profile of the amplified beam and address interference fringes observed in the beam. These adjustments will undoubtedly improve the geometry of the trapped atom cloud, and provide a cleaner space within which ultra-cold plasma dynamics can be investigated.

While further work will improve the experimental results, the tapered amplifier has been successful in opening a new parameter space within which ultra-cold plasmas can be studied at Colby College. The device has facilitated the creation of trapped atom samples with densities over ten times the maximum previously achieved, a result that is expected to be expanded as an understanding of the amplifier and its effects builds. With this development comes a new era of plasma research at Colby College. Hopes are high that the new freedom afforded by the tapered amplifier will allow ultra-cold plasmas in the Tate Lab to be studied with unprecedented depth and detail.

APPENDICES

APPENDIX 1 DERIVATION OF MOT NUMBER DENSITIES

The number density of samples in the MOT can be inferred using measurements of the fluorescence power from the $5S_{1/2} \rightarrow 5P_{3/2}$ cooling transition as well as spatial measurements from the Linear Diode Array (LDA).

Figure A.1 shows a schematic for the measurement of the florescence power of the MOT. Knowing the geometry of the trap, the measured power can be related to the total power according to

$$P_{measured} = \frac{\Omega}{4\pi} P_{total} = \frac{\pi d^2/4}{4\pi l^2} P_{total} = \frac{d^2}{16 l^2} P_{total}, \qquad \text{(A.1)}$$

where Ω, d and l are defined in Figure A.1, and P is the fluorescence power from the trapped sample. The fluorescence power can be described using the photon energy $h\upsilon$ by

$$P_{total} = h\upsilon N = h\upsilon \frac{N_{atom}}{2\Gamma}, \qquad \text{(A.2)}$$

where υ is the frequency of the fluorescence photons, N is the number of photons received per

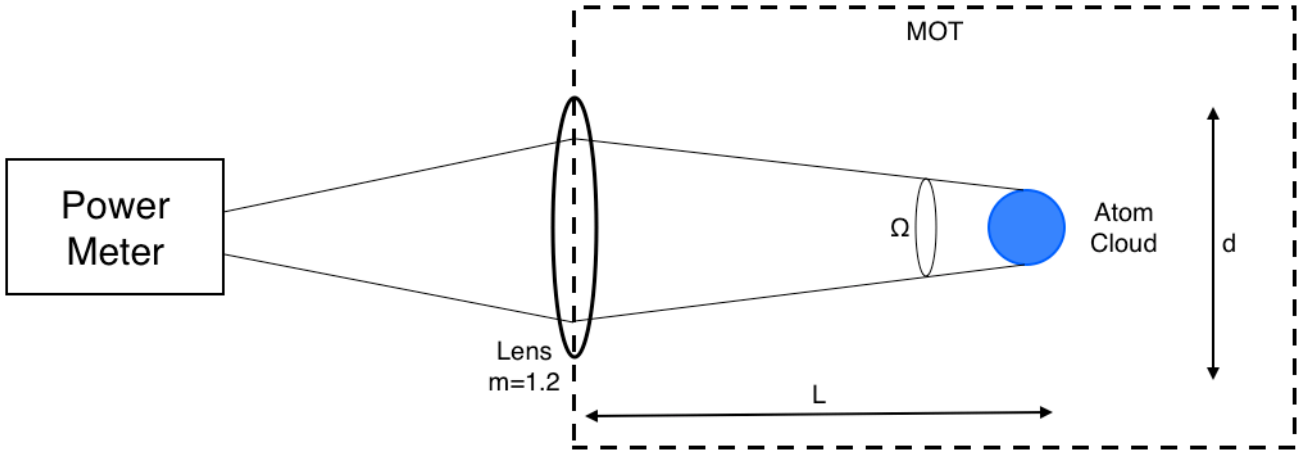

Figure A.1: Shows the geometry of the MOT with relation to the measurement of the fluorescence power.

second, N_{atom} is the number of atoms in the trapped cloud, and Γ is the lifetime of the 5p state in the cooling transition. Equations A.1 and A.2 can be combined and solved for N_{atom} to show

$$N_{atom} = \frac{4\pi}{\Omega}\frac{2\Gamma}{h\upsilon}P_{measured} = (6.47\times10^{7})P_{measured}\,. \qquad \text{(A.3)}$$

Thus, the measured optical power of the transition florescence has been related to the total number of trapped atoms. Note that $P_{measured}$ is assumed to have units of microwatts in equation A.3.

To determine the density of the trapped sample, it is necessary to convert the measurement from the LDA, which is in terms of time, to a spatial value. Using the geometry of the detector, can translate the full width at half maximum (FWHM) of the LDA signal to a spatial FWHM (Δ_{im}) according to

$$\Delta_{im} = \frac{FWHM_{measured}}{12.5\ (ms)}28.6(mm). \qquad \text{(A.4)}$$

Noting that the measurement from the diode array is made through a lens, a simple multiplicative constant ($m=1.2$, the imaging system's lateral magnification) can convert the image FWHM, Δ_{im}, to the object FWHM Δ_{ob}. Now, to determine true spatial dimensions for the trapped cloud, it is necessary to assume that the cloud follows a Gaussian spatial profile

$$e^{-r^2/2\sigma^2}\,. \qquad \text{(A.5)}$$

Knowing that this distribution is ½ when $2r=\Delta_{ob}$, the equation can be solved to show

$$\Delta_{ob} = 2\sqrt{2\ln(2)}\sigma. \qquad \text{(A.6)}$$

With knowledge of the parameter σ, can write the complete Gaussian number density distribution

$$n_i(r) = \frac{N_{atom}}{(2\pi\sigma^2)^{\frac{3}{2}}}e^{-\frac{r^2}{2\sigma^2}}, \qquad \text{(A.7)}$$

where σ is defined as in equation A.5. Setting $r=0$ in A.7, gives the maximum number density

$$n_{max} = \frac{N_{atom}}{(2\pi\sigma^2)^{\frac{3}{2}}} = \frac{(6.47\times10^7)P_{measured}}{(2\pi\sigma^2)^{\frac{3}{2}}}. \qquad \text{(A.8)}$$

Equation A.7 can also be used to find the average number density

$$n_{avg} = \frac{N_{atom}}{(4\pi\sigma^2)^{\frac{3}{2}}} = \frac{(6.47\times10^7)P_{measured}}{(4\pi\sigma^2)^{\frac{3}{2}}}. \qquad \text{(A.9)}$$

Thus the maximum and average number densities of samples confined in the MOT have been written as a function of measured results.

APPENDIX 2 TA OPERATION

The tapered amplifier can be operated entirely from the ITC 4000 controller box. However, before turning on the TA, it may be necessary to turn on the shutter controller box to ensure the shutter interlock is active. To turn on this box, turn the power to "On" and ensure the control switch is set to "Comp." To turn on the TA, simply turn hit the "LD ON" button on the ITC 4000 box. Shortly after doing this, the shutter should release, allowing the seed laser into the TA. If the shutter does not automatically do this, it may be necessary to release it manually by toggling the control switch to the "Manual" setting. The amplifier's operation can be quickly verified by looking for brightness fluctuations in the output when in the input is blocked and unblocked.

The TA can occasionally become slightly misaligned, which diminishes the output power. To realign, place a power meter immediately after the TA. While watching the power meter, *carefully* move the translational adjustments on the aspherical lens mount on the input side of the TA housing to maximize the output power. Once this is maximized, the last PCBS in the optical array before the TA can be finely adjusted to again maximize the output power.

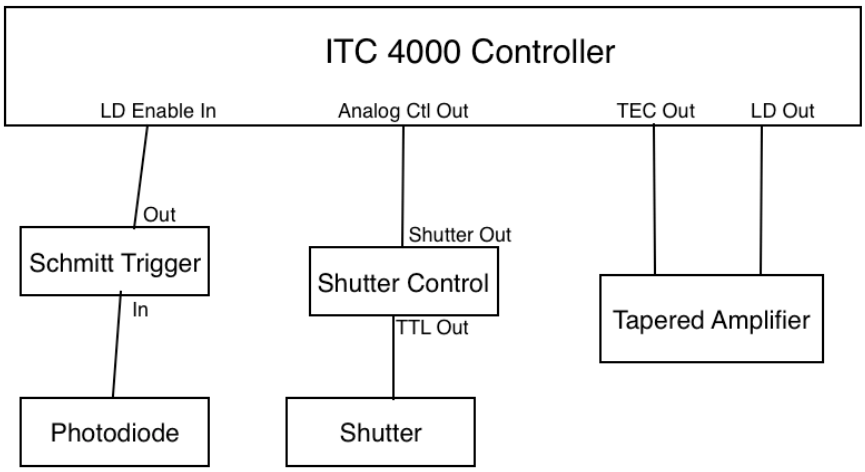

Figure A.2: Shows the connections between the ITC 4000 controller box and TA components.

Figure A.2 shows a schematic of the connections between the TA, ITC 4000, and interlock mechanisms. Additionally, several of the interlocks rely on internal programming within the ITC 4000 box. To ensure they function correctly, both the "Temp. Protection Mode" and "Inhibit Input Mode" with the "LD Output Configuration" menu should be set to "Protection." This setting will stop the TA output and activate the interlocks if anything goes wrong with the input beam or temperature readings.

As a final note, the shutter is driven by the "Analog CTL Out" output on the ITC 4000. This output delivers a voltage to the shutter proportional to the current driving the TA. For this reason, the shutter does not function correctly when the TA is operated below 0.9 A. Additional external electronics will be required to fix this limitation.

APPENDIX 3 POWER CALIBRATION DATA

Extensive data was taken throughout the project to understand the power output of the tapered amplifier. Referring to Figure 5.1, the input power to the TA is adjusted using the λ/2 plate and PCBS nearest to the TA in the path of the seed beam. Additionally, the TA output power is contingent on the input power and the current driving the amplifier. The following tables show the power and current values used throughout in this thesis.

As a note, the optical isolator after the TA transmits a certain percentage of the TA output (usually ~75%), so measurement of the output power that is sent to the MOT should be made after this optical component. Additionally, the values quoted in this section are known to change significantly as the TA alignment degrades. If precise knowledge of the cooling laser power is necessary, new calibration data should be taken before use of the MOT.

TA Current (A)	1/2 Wave Plate Setting	Post-OI Optical Power (mW)
0.99	172	101
1.14	172	160
1.31	172	239
1.47	172	320
1.63	172	402
1.79	172	486
2	172	570

Table A.1: Shows the optical powers of the TA measured after the OI for a number of driving currents.

TA Current (A)	1/2 Wave Plate Setting	TA Input Power (mW)	TA Output Power (mW)*	TA Current (A)	1/2 Wave Plate Setting	TA Input Power (mW)	TA Output Power (mW)*
0.7495	158	0.455	9.86	1.4995	158	0.455	51.4
0.7495	160	1.09	12	1.4995	160	1.09	71.9
0.7495	162	2.84	15.5	1.4995	162	2.84	124
0.7495	164	5.14	19.9	1.4995	164	5.14	168
0.7495	166	8.64	27	1.4995	166	8.64	238
0.7495	168	12.3	33.7	1.4995	168	12.3	298
0.7495	170	18	41.1	1.4995	170	18	341
0.7495	172	22.9	48.6	1.4995	172	22.9	410
0.9995	158	0.455	19.1	1.7496	158	0.455	83.1
0.9995	160	1.09	25.1	1.7496	160	1.09	104
0.9995	162	2.84	35.4	1.7496	162	2.84	195
0.9995	164	5.14	51.8	1.7496	164	5.14	232
0.9995	166	8.64	71.7	1.7496	166	8.64	335
0.9995	168	12.3	92.9	1.7496	168	12.3	440
0.9995	170	18	114	1.7496	170	18	471
0.9995	172	22.9	130	1.7496	172	22.9	570
1.2495	158	0.455	31.8	1.995	158	0.455	125
1.2495	160	1.09	45.7	1.995	160	1.09	155
1.2495	162	2.84	73.5	1.995	162	2.84	250
1.2495	164	5.14	110	1.995	164	5.14	362
1.2495	166	8.64	142	1.995	166	8.64	402
1.2495	168	12.3	181	1.995	168	12.3	512
1.2495	170	18	217	1.995	170	18	623
1.2495	172	22.9	256	1.995	172	22.9	741

Table A.2: Calibration data for the optical power both before and after the TA as a function of both the half-wave plate setting and TA driving current.

REFERENCES

[1] NASA Office of Science Education. 2015. “Dark Energy, Dark Matter.” *NASA Office of Science Education*. Accessed April 21, 2015. http://science.nasa.gov/astrophysics/focus-areas/what-is-dark-energy/

[2] Southwest Research Institute. 2015. “Plasma: The Fourth State of Matter.” *Southwest Research Institute*. Accessed April 21, 2015. http://pluto.space.swri.edu/image/glossary/plasma2.html.

[3] Kross, Brian. 2015. “Questions and Answers: What Is Plasma?” *Jefferson Lab Office of Science Education*. Accessed April 20, 2015. http://education.jlab.org/qa/plasma_01.html.

[4] Killian, Thomas C., and Steven L. Rolston. 2010. “Ultracold Neutral Plasmas.” *Physics Today* 63: 46–51. doi:10.1063/1.3366240.

[5] Fuchs, Matthias. 2006. “Development of a High Power Stabilized Diode Laser System.” University of Oregon.

[6] Kangara, Jayampathi. 2012. “Design and Construction of Tapered Amplifier Systems for Laser Cooling and Atom Trapping Experiments.” Miami University.

[7] Maguire, LP. 2004. “High Performance Laser Shutter Using a Hard Disk Drive Voice-Coil Actuator.” *Review of Scientific Instruments* 75: 3077–79. doi:10.1063/1.1786331.

[8] Demarco, Brian. 2001. “Quantum Behavior of an Atomic Fermi Gas.” University of Colorado.

[9] Voigt, D., E. C. Schilder, R. J. C. Spreeuw, and H. B. Van Linden Van Den Heuvell. 2000. “Characterization of a High-Power Tapered Semiconductor Amplifier System” *Applied Physics Letters B* 284: 6. doi:10.1007/s003400100513.

[10] Kowalski, Krzysztof *et al.* 2012. "Magneto-Optical Trap: Fundamentals and Realization." *Computation Methods in Science and Technology* 2: 115-129. doi: 10.12921/cmst.2010.SI.02.115-129

[11] Metcalf, H.J. and P. van der Straten. 2003. "Laser cooling and trapping of atoms," *Journal of the Optical Society of America B.* 20, 887-908.

[12] Wikipedia contributors. "Gain." *Wikipedia, The Free Encyclopedia.* Accessed May 4 2015. http://en.wikipedia.org/w/index.php?title=Gain&oldid=651150662